THE JOURNAL OF PHYSICAL CHEMISTRY B

Article

pubs.acs.org/JPCB

Surface Graft Configuration Dependency of the Morphologies of Heterosurface Sheet Polymers

Minwoo Han and Eunji Sim*

Department of Chemistry and Institute of Nano-Bio Molecular Assemblies, Yonsei University, 50 Yonsei-ro Seodaemun-gu, Seoul 120-749, Korea

ABSTRACT: Using dissipative particle dynamics, we investigated the graft configuration-dependent scroll formation of sheet polymers and their morphologies. Two types of coarse-grained graft disorder models were considered at various displaced tether fractions. Although tether coils were identical, sheet anisotropy arose from discrepancies in graft configurations on the two opposite-side surfaces and resulted in spontaneous scroll formation. An anisotropy parameter based on the relative free volumes of tether coils was introduced and shown to be linearly related to the radius of gyration. This demonstrates that sheet anisotropy, and consequently internal cavity diameters of tubular scrolls, can be regulated by surface grafting. We also examined a coassembly of laterally grafted rod−coil amphiphiles as an alternative way to form sheet polymers with heterosurfaces. The coassembly of conformation mismatching rod−coil molecules is expected to form anisotropic bilayers, as each layer is assembled independently with different degrees of graft disorder. We believe this work provides a framework for further research regarding morphology control by surface grafts of sheet polymers.

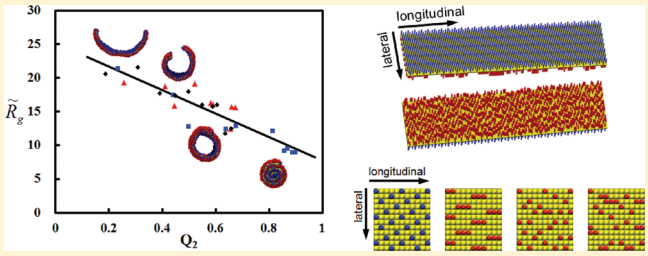

I. INTRODUCTION

Until recently, vesicles have been the focus of drug delivery vehicle development due to the presence of internal cavities.[1−4] Spheres, however, have the smallest surface areas of all of the possible structures, whereas large contact areas are useful for surface modification of carriers' functionalities, including targeting. Moreover, the chemical and physical properties of spheres, including the kinetics, diffusivity, target selectivity, and functionality, are determined by only one factor, the size of the vesicle. It is therefore desirable to take advantage of structures with larger surface areas, such as tubular scrolls. Tubular scrolls also have additional geometric degrees of freedom, including tubule (external) diameter and tubule length, which affect their properties. For example, mechanical movement is governed by tubule length and diameter, whereas some properties, such as the encapsulant time-release profile, are known to depend closely on internal cavity diameter and scroll length.[5,6] Growing interest in drug delivery vehicles has prompted extensive investigation into nanosized tubular scrolls such as carbon nanotubes, in both experimental[6−14] and theoretical[15−17] studies. Despite their potential, the fabrication of tubular scrolls, especially using bio-/organic materials that may be naturally biocompatible and bioabsorbable, is not straightforward. Although regulation of the internal cavity is crucial for biomedical applications,[10,12,18] the fundamental understanding of scroll formation and the systematic manipulation of internal cavities is lacking and is, in large part, yet to be explored.

It has been shown that anisotropy in two-dimensional (2D) sheets causes various curved phases, including tubular scrolls.[15−17] There have been extensive studies on 2D sheet polymers, that is, polymers with 2D connectivity. Examples of 2D sheet polymers include carbon nanotubes,[19,20] graphene,[21] graphite oxide sheets,[22,23] polymerized layers,[24,25] and self-assembled membrane structures.[26,27] In addition, various simulations using Dissipative Particle Dynamics (DPD),[28] Brownian Dynamics,[29] Molecular Dynamics (MD),[27] and Monte Carlo simulation methods[16] have been employed to explore 2D sheet morphology. Recently, we have reported tubular scroll formation with controlled internal cavities by purposely breaking the chemical and volume symmetries of surface grafted coils.[28] DPD simulations showed that modification of the tether coil properties of rod−coil amphiphiles is relatively simple yet highly effective for inducing various types and degrees of sheet anisotropy. The fundamentals of the DPD algorithm are equivalent to those of MD simulations. The use of a coarse-grained model, however, enables computations roughly 10^4−10^7 times more efficient than those of all-atom MD simulations by replacing a group of atoms with a single coarse-grained bead.[30] In general, the computation amount to calculate the energy or force for a system of N particles scales as N^2 or $N^{3/2}$. Moreover, the propagation time step, which scales as $\Delta t = l(m/kT)^{1/2}$, can also be enlarged because a particle becomes larger in diameter and heavier in mass for the coarse-grained model. Because a single soft sphere replaces several atoms, the interaction schemes between particles will also become simpler than all-atom models. For instance, the number of bonds will decrease, and some angle constraints may be omitted allowing additional

Received: January 30, 2012
Revised: April 8, 2012
Published: May 7, 2012

savings. Nanosized tubular scrolls are often developed in the condensed phase, in which environmental properties significantly affect the morphology. Therefore, the use of the DPD method is appropriate because it can correctly describe hydrodynamic effects, which are critical in the condensed phase dynamics found in solid states or solutions.[30,31]

In this Article, we explore the influence of the tether coil graft configuration on polymer morphology and, more importantly, seek to determine the driving force of the spontaneous transformation of a flat membrane into a scroll. The coassembly of laterally grafted rod−coil molecules is also discussed as an alternative system to produce tubular scrolls with controlled internal cavities. A brief description of the DPD simulations and the coarse-grained model is presented in section II. In section III, the transformation of surface grafted sheet polymers is explored with respect to graft configuration disorder. Concluding remarks appear in section IV.

II. METHODS

A bare sheet polymer was prepared adapting the sheet model described in ref 28, followed by surface grafting. As is schematically drawn in Scheme 1a and b, tether coils (five beads in a flexible chain) on the reference side were grafted at the reference graft points, which had well-defined pseudohexagonal configurations. On the reverse side, a fraction of the tether coils were displaced from their ordered reference graft points to construct a disordered graft configuration (red beads in Scheme 1c−f). Two types of displacement models were considered. For model I (Scheme 1d), maximum overlap is imposed between tether coils on neighboring lateral lines. Once a lateral line is randomly chosen, all tether coils on the line are shifted such that they are grafted next to tether coils on the previous line. For model II(d) (Scheme 1e, d = 1 and (f) d = 2), any chosen tether coil can be displaced along the lateral direction. Once a tether coil is randomly chosen, it is displaced by d sheet beads to the left or right of the original graft point by another random number.

Scheme 1. Initial Configurations of Coarse-Grained Surface-Grafted Sheet Polymer[a]

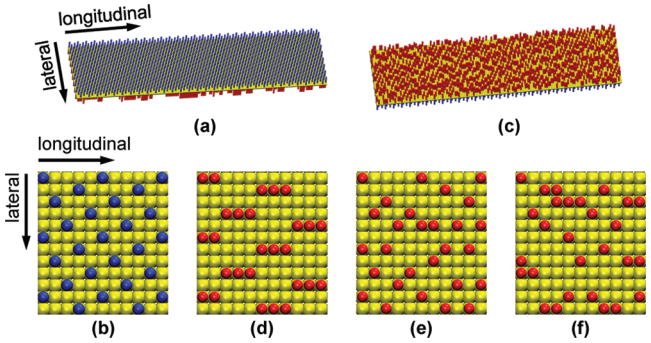

[a](a) The reference surface side with its augmented top view of reference graft points in (b), (c) a disordered surface side with augmented top views of displaced graft points according to (d) Model I, (e) Model II(1), and (f) Model II(2), respectively. Blue beads denote the reference graft points of tether coils, while red beads represent graft points on the disordered surface. Yellow beads are sheet beads.

In DPD, interactions between any two types of sheet (R), coil (C), and solvent (S) beads are described by a soft repulsive potential as $F_{ij}^{c} = a_{ij}(1 - r_{ij}/r_c)\hat{r}_{ij}$, $r_{ij} = |r_{ij}\hat{r}_{ij}| \leq r_c = 1$ for particles i and j.[30] The parameter $a_{ij}(i,j$ = R,C,S) describes the strength of the repulsive force; a_{ii} is for a homogeneous interaction between the same types of beads and is set as $a_{ii} = 25k_BT$, while a_{ij} $(i \neq j)$ is for a heterogeneous interaction between different types of beads (Table 1). Surface grafted polymer sheets transform to various cylindrical structures due to broken symmetry in the solvent affinities and/or volumes of surface tether coils.[28] On the contrary, isotropic sheet polymers remain flat. In this Article, all of the properties of coil beads are modeled as identical regardless of the surface sides to isolate the role of surface grafting. In addition, a theta solvent condition was chosen for coil beads, that is, $a_{CS} = 25k_BT$, such that scroll formation due to coil−solvent repulsion and/or coil−coil attraction became irrelevant. The theta solvent is a solvent in which polymer segments act like ideal chains, and, thus, the conformations adopted by polymers dissolved in theta solvents are identical to those in bulk phase. Here, the theta solvent for the coil beads was chosen for two major reasons: first, the theta solvent molecules mimic the surface coils of surrounding polymer sheets in bulk phase. Second, the influence of the coil−solvent interaction is excluded, and, thus, spontaneous scrolling occurs strictly due to sheet anisotropy caused by graft disorder. Clearly, graft conformation is affected by polymer−solvent interaction; however, the measured characteristics of polymer structures, such as its morphology, become independent of the solvent when a theta solvent is used. Dependence of solvent properties on scroll formation is not explicitly discussed here but can be found elsewhere.[28]

The aspect ratio (short side-lateral:long side-longitudinal) of the sheet model was chosen to be 4:15. A surface grafted sheet polymer was placed inside a simulation box, which was filled with single bead solvent molecules. The total number of beads in the simulation box was 384 000−600 000, including solvent beads; that is, the number density of the system was $\rho = 3$. All simulations were performed with the LAMMPS package[32] with time step $\Delta t = 0.02\tau$, and the temperature was maintained at 0.3 in DPD reduced units.[30] VMD was used for visualization.[33] Details of the DPD method can be found elsewhere.[28,30,31,34]

III. RESULTS AND DISCUSSION

A. Heterosurface Sheet Polymers. As presented in Figure 1, all models spontaneously scrolled into curved structures at

Table 1. DPD Potential Parameters[a]

tether coil					sheet					
$a_{\alpha\alpha}$[b]	a_{CS}[b]	a_{RC}[b]	k_{coil}[c]	$\bar{r}_{coil}$[c]	a_{RS}[b]	k_{lat}[c]	k_{long}[c]	$\bar{r}_{lat}$[c]	$\bar{r}_{long}$[c]	k_{arg}[d]
25	25	30	25	0.5	30	100	50	0.5	0.5	20

[a]In subscripts, C, R, and S correspond to tether coils, sheets, and solvents, respectively. $a_{\alpha\beta}$ is in units of k_BT, and other parameters are in DPD reduced units. [b]DPD repulsion parameter, α = C,R,S. [c]Harmonic bonding, $V_{bond}(r) = 1/2k_{bond}(r - \bar{r}_{bond})^2$, for coil chain (coil) and lateral(lat)/longitudinal(long) sheet direction. [d]Soft angle constraint, $V_{ang}(\theta) = k_{ang}(1 + \cos\theta)$.

dx.doi.org/10.1021/jp300968c | J. Phys. Chem. B 2012, 116, 5771−5776

Figure 1. Cross sections of DPD-simulated surface-grafted sheet polymers along the longitudinal direction for models I, II(1), and II(2) with respect to tether coil displacement fractions (χ).

various displacement fractions of tether coils (χ). For a given χ, model I generally resulted in structures with the highest curvatures or the smallest internal cavities. Scroll curvature depends rather systematically on χ, even monotonically for models I and II(1). While tether coils at reference graft points can have the largest free volumes among their surrounding neighbors, displaced ones may be located near other tether coils, producing a large overlap, that is, entropic repulsion. Scheme 2 illustrates the coil−coil overlap caused by the graft disorder depending on the model. The open circles represent sheet beads, and the shaded area denotes free volume required for a tether coil to expand. For models I and II(1), as more tether coils were displaced from their reference graft points, greater entropic repulsion was induced on the disordered side. On the contrary, the coil−coil overlap of model II(2) increases up to $\chi \approx 0.7$. As more coils are displaced, however, it is clearly visible that the coils overlap less. Regardless of the model, the disordered graft configuration leads to asymmetry in surface entropy, which, in turn, gives rise to overall sheet anisotropy for scroll transformation.

Scheme 2. Schematic Illustration of the Coil−Coil Overlap Depending on the Graft Disorder Model and Tether Coil Displacement Fraction (χ)[a]

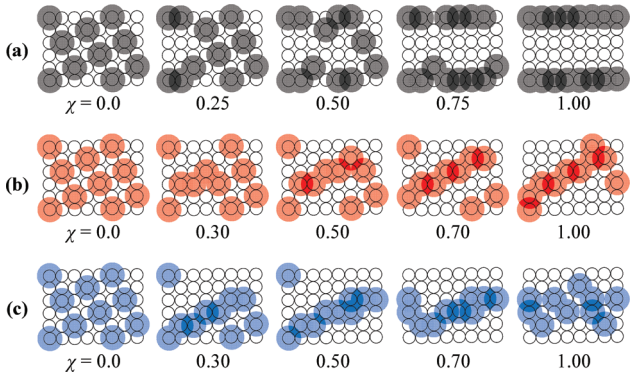

[a](a) Model I, (b) Model II(1), and (c) Model II(2). While the circles represent sheet beads, the shaded area denotes the free volume required for a tether coil to expand.

Hence, by comparing relative free volumes of the tether coils on the two surfaces, the degree of sheet anisotropy can be represented quantitatively. Consider the anisotropy parameter:

$$Q_\alpha = 1 - \frac{[f_\alpha]_{dis}}{[f_\alpha]_{ref}} = 1 - \frac{[\bar{R}_C^{\alpha} - D_{eff,C}^{\alpha}]_{dis}}{[\bar{R}_C^{\alpha} - D_{eff,C}^{\alpha}]_{ref}} \quad (1)$$

where $f_\alpha = \bar{R}_C^{\alpha} - D_{eff,C}^{\alpha}$ is the free volume of the tether coils, $[]_{ref}$ and $[]_{dis}$ denote properties of the reference and disordered surface sides, respectively, $\bar{R}_C$ is the average nearest-neighbor distance between tether coils in the longitudinal direction, that is, the rolling direction, and $D_{eff,C}$ is the effective diameter of a single tether bead. In other words, $\bar{R}_C$ describes the graft configuration, while $D_{eff,C}$ represents properties of the tether coils. $[\bar{R}_C]_{ref}$ is a well-defined constant due to ordered graft configuration, whereas $[\bar{R}_C]_{dis}$ depends on graft point disorder. For models discussed in this Article, $[D_{eff,C}]_{ref} = [D_{eff,C}]_{dis}$ because $D_{eff,C}$ depends on the coil−solvent affinity and the theta solvent condition was applied. When $D_{eff,C}$ is smaller than $\bar{R}_C$, the tether coils have enough free space and exert no significant entropic repulsion on the sheet. In contrast, if $D_{eff,C}$ is larger than $\bar{R}_C$, the tether coils are overcrowded and cause large entropic repulsion. Accordingly, the ratio of f_α describes the relative strength of the entropic repulsion due to heterogeneous surface grafting. By definition, $Q_\alpha = 0$ indicates an isotropic sheet polymer, and Q_α deviates further from zero in the case of higher degrees of sheet anisotropy. Depending on the exponent, Q_α represents the degree of sheet anisotropy in terms of a tether coil's effective diameter ($\alpha = 1$), area ($\alpha = 2$), and volume ($\alpha = 3$). Here, $\alpha = 2$ was chosen for further investigation because overlap area near surfaces affects the overall entropic repulsion most significantly. Variations of Q_2

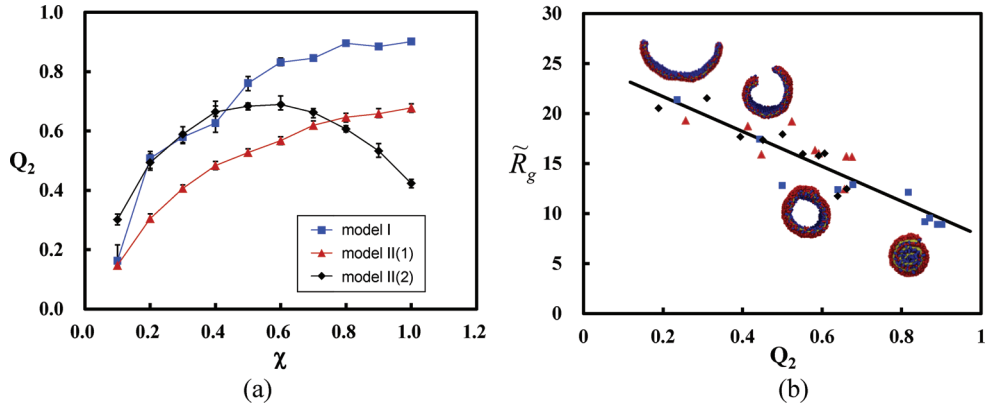

Figure 2. (a) The tether coil displacement fraction (χ)-dependent anisotropy parameter (Q_2) and (b) the relationship between Q_2 and the radius of gyration ($\tilde{R}_g$). At a given χ, error bars represent minimum and maximum values of Q_2 out of 50 randomly generated graft configurations. In some cases, error bars are smaller than markers. While lines in (a) are arbitrarily drawn to guide, the solid line in (b) is a linear regression fit, $\tilde{R}_g = -17.44Q_2 + 25.18$.

dx.doi.org/10.1021/jp300968c | J. Phys. Chem. B 2012, 116, 5771−5776

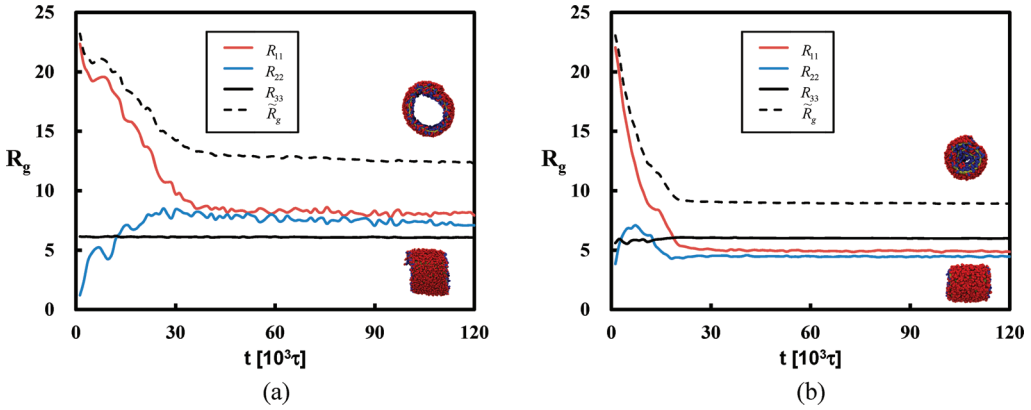

Figure 3. Time evolution of the radii of gyration, $\tilde{R}_g$ (dashed line), and three principal radii, R_{ii} (solid lines), for model I at (a) $\chi = 0.4$ and (b) $\chi = 0.9$. While $R_{33} \equiv R_{lat}$ is invariant and denotes the lateral dimension of the sheet model, $R_{11} \approx R_{22}$ represents the tubule diameter, which is proportional to that of the internal cavity.

with respect to χ are shown in Figure 2a for the three models discussed above. In general, Q_2 systematically depends on the displacement fraction χ for a given disorder model. Each data point indicates the average Q_2 along its minimum and maximum values of more than 100 randomly generated graft configurations.

We also explored the relationship between the degree of sheet anisotropy and the morphology. Details of the morphologies and scrolling processes of sheet polymers were investigated through the radius of gyration ($\tilde{R}_g$), which was evaluated from snapshots taken at $\sim 4.8 \times 10^4\tau$ of each simulation. In Figure 2b, a strong correlation of Q_2 and $\tilde{R}_g$ is clearly visible. $\tilde{R}_g$ varies almost linearly with Q_2, indicating that tether coil overlap is indeed the governing factor in sheet anisotropy. A linear regression fit was obtained as $\tilde{R}_g = -17.44Q_2 + 25.18$ with the coefficient of determination $R = -0.9101$. Because the length of the tubule is roughly the same as the sheet's lateral dimension, as shown in Figure 3, a large $\tilde{R}_g$ value implies a large tubule diameter and, in turn, a large internal cavity. This implies that sheet polymers with regulated graft configurations can indeed produce tubular scrolls with controlled internal cavities.

The fabrication of sheet polymers with heterogeneous surface grafts, that is, heterosurfaces, has been of interest for biomedical applications such as drug delivery vehicles and tissue engineering.[35−37] As far as the authors are aware of, however, there has been no relevant experiment in which scroll formation dependence on graft disorder was explicitly investigated. Nevertheless, membrane bending due to the introduction of foreign objects such as proteins or short rods into a flat membrane may be related to the principles discussed here.[38,39] The entropic repulsion asymmetry driven by surface graft disorder imitates the area discrepancy due to inserted objects, because such disturbance causes sheet anisotropy and eventually makes the flat sheet bend. We believe that this work will help efforts to transform sheet polymers with heterosurfaces into well-defined morphologies that can be directly used in diverse applications. Significant work remains to be performed to determine how bonding topology, aspect ratio, and/or types of molecular component chemical properties influence sheet morphology.

B. Coassembly of Laterally Grafted Rod−Coil Amphiphiles. In the previous subsection, how spontaneous scroll formation depends on graft disorder was discussed. In fact, the fundamental principles of the scroll formation can be easily extended to various experimental systems. As long as there is a way to construct a bilayer structure whose surface is covered with asymmetric grafts, one can anticipate its subsequent scrolling. Hence, as an alternative way of constructing a polymer-based heterosurface sheet, we propose the coassembly of block copolymers. This subsection focuses on the potential formation of disordered surface grafts by explicitly investigating molecular arrangements within coassembled clusters rather than their secondary morphological changes.

Recently, laterally grafted copolymers have been made to self-assemble into a wide variety of complex geometries.[14,28,29,40] A laterally grafted rod−coil amphiphile (GRC) is a branched polymer composed of a main chain with one or more substituent side chains. In particular, T-shaped rod−coil amphiphiles (T-GRC), in which flexible tether coils are grafted at the middle of a rigid rod, are reported to form a long-range ordered 2D bilayer, an analogue of a surface grafted sheet polymer.[14,41] The main driving force for T-GRC aggregation is $\pi-\pi$ stacking among neighboring aromatic rods, whereas flexible tether coils provide configuration entropy, prohibiting the close approach of other coils. As a consequence, in the initially aggregated layers, rod orientation is ordered in a short-range without well-defined tether coil orientation or configuration. Subsequent rearrangements within the layer occur to achieve a thermodynamically favored free-energy minimum structure, in which rods are organized parallel to each other and tether coils are arranged to have a hexagonal configuration.

By perturbing the isotropic layer formation of T-GRC self-assembly, anisotropic bilayers may be obtained. Let us consider a coassembly of T-GRCs with an asymmetrical structural isomer (A(d)-GRCs), for which the molecular component is equivalent to T-GRC except that the tether coil is grafted at d beads off the middle of the rod. To investigate the possible formation of disordered layers and to visually illustrate molecular arrangements and graft configurations, MD simulations were employed on coarse-grained rod models in a periodic 2D box. Despite its simplicity, 2D MD simulation is ideal for demonstrating the progress of layer formation, including grafted rods' rearrangements, which occur on the surface of aggregated GRC layers. Lennard-Jones (LJ) potential was used to mimic $\pi-\pi$ interactions between the aromatic rods of GRCs. Harmonic bond potentials and soft angle constraints were employed to model the rod, which consisted of five beads. The tether coil was replaced by a single bead at the graft point embedded in the rod and is depicted as a red bead in Figure 4.

dx.doi.org/10.1021/jp300968c | J. Phys. Chem. B 2012, 116, 5771−5776

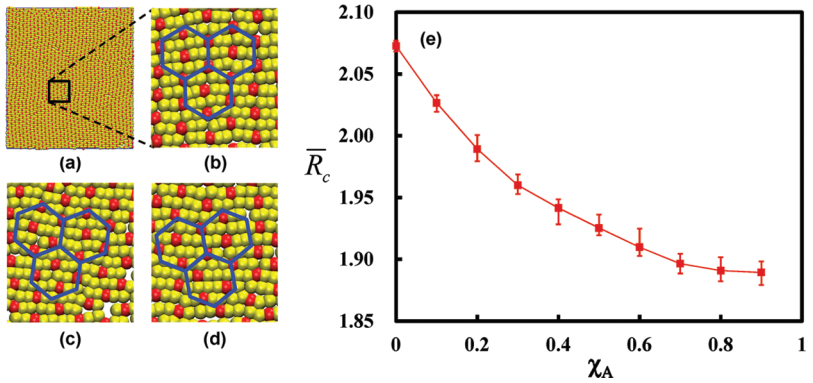

Figure 4. MD-simulated structures of T-GRC and A(1)-GRC coassembly at (a) the A(1)-GRC fraction, (b) $\chi_A = 0$, (c) $\chi_A = 0.2$, and (d) $\chi_A = 0.4$. Tether coil graft points are denoted as red beads, while yellow beads are rod beads and the blue hexagons in (b)−(d) are drawn for comparison. (e) Nearest-neighbor tether coil distances in the longitudinal direction, $\overline{R}_C$: at a given χ_A, the marker represents the average $\overline{R}_C$ taken from 10 independent initial structures, and error bars correspond to minimum and maximum values of $\overline{R}_C$ within the ensemble. The solid line is arbitrarily drawn to guide.

Tether beads repel each other through soft repulsive potentials. Model potential parameters are listed in Table 2. All

Table 2. MD Potential Parameters in Lennard-Jones Reduced Units

$\varepsilon_{LJ}{}^a$	$\sigma_{LJ}{}^a$	$\kappa_{cc}{}^b$	$r_{cc}{}^b$	$\kappa_{bond}{}^c$	$\overline{r}_{bond}{}^c$	$\kappa_{ang}{}^d$
1.0	1.0	5.0	2.5	100	0.9	20

[a]Lennard-Jones inter-rod interaction. [b]Coil−coil repulsion, $V_{cc}(r) = \kappa_{cc}[1 + \cos(\pi r/r_{cc})]$, $r < r_{cc}$. [c]Harmonic intrarod bonding. [d]Intrarod soft angle constraint.

simulations were performed in a 2D simulation box with a size of $(80 \times 80)\sigma_{LJ}^2$ with 1300 rods, with the time step $\Delta t = 0.001\tau$, and at the constant temperature $T = 0.7T^*$ in LJ reduced units.[30] The Velocity Verlet algorithm was used along with a Nosé−Hoover thermostat.

For isotropic T-GRCs, the minimum free-energy structure was indeed well ordered. As shown in Figure 4a and b, T-GRCs were arranged into an ordered layer with a hexagonal tether coil configuration. Examples of T-GRC and A(1)-GRC coassembled layers, in which the hexagonal arrangements of tether beads are disturbed, are shown in Figure 4c and d. In fact, a layer formed by the coassembly of T-GRC and A(d)-GRC is equivalent to the previously discussed model II(d) surface grafted sheet polymer. Because of the similarity of the molecular components, intermolecular interactions between heterogeneous GRCs should be almost indistinguishable from those between homogeneous GRCs. Aggregation in the GRC mixture will still be driven by $\pi-\pi$ stacking and result in a disordered initial layer. Unlike in T-GRC self-assembly, however, the asymmetric conformation of A(d)-GRCs impedes the progress of tether coil rearrangements. In relation to protein folding dynamics, rearrangements within the sheet polymer can also be viewed in terms of energy landscapes.[42] A disordered GRC coassembled layer has a large number of configuration states available and thus fewer states to the ordered counterpart. If the time required for the layer to attain its global minimum conformation is large, it is called kinetically trapped. The local roughness of the energy landscape reflects kinetic traps, corresponding to the accumulation of partially ordered intermediates. The branching of polymer chains and indistinguishable molecular interactions affects the abilities of chains to slide past one another. Therefore, collective rearrangements are rare events with high energy costs. Consequently, the GRC coassembled layer will be kinetically trapped. This kinetic trap prohibits the polymer layer from attaining the most thermodynamically stable configuration with perfectly ordered GRCs: as a result, an amorphous glassy distribution of tether coils largely remains. For the same reason, the phase separation of T-GRC and A(d)-GRC is unlikely to occur.

The local roughness of the energy landscape was examined indirectly through variations of the $\overline{R}_C$ values of MD-simulated T-GRC and A(1)-GRC coassembled surfaces. For a given A(1)-GRC fraction, χ_A, 10 randomly generated initial structures were simulated. The average $\overline{R}_C$ value and its range of variation are shown in Figure 4e. T-GRC self-assembly ($\chi_A = 0$) clearly led to the largest $\overline{R}_C$ with the lowest range of variation, while average $\overline{R}_C$ values and their ranges changed systematically with χ_A, implying perturbed surface formation due to A(1)-GRC insertion. Each layer is assembled independently, it is highly likely that bilayers with heterosurfaces are formed. Therefore, we envision that GRC coassembly will lead to a formation of metastable yet long-lived anisotropic layers that spontaneously transform to curved structures, including tubular and filled scrolls. Furthermore, the systematic control of scroll morphology through the manipulation of the mixture compositions and of GRC molecular conformations appears promising.

IV. CONCLUDING REMARKS

The graft configuration-dependent scroll formation of sheet polymers was explored using DPD and MD simulations on coarse-grained models. Spontaneous rolling of the model sheet polymer was observed by inducing anisotropy via heterogeneous surface grafting. It was also found that, by manipulating graft disorder, tubular scrolls with controlled internal cavities, which are highly desirable for drug delivery vehicles, can be constructed. The driving force for scroll transformation was discussed in terms of the anisotropy parameter, which is based on the relative free volumes of tether coils. Motivated by recent works on laterally grafted rod−coil amphiphiles, we also suggested the coassembly of block copolymers as an alternative means of forming anisotropic bilayers, which will eventually transform into tubular scrolls. The idea was verified by MD simulations that successfully demonstrated the formation of kinetically trapped disordered layers. We believe that this

dx.doi.org/10.1021/jp300968c | J. Phys. Chem. B 2012, 116, 5771−5776

Article provides not only a fundamental understanding of sheet to scroll transformation but also a framework for further research regarding morphology control by surface grafting of 2D sheet polymers.

AUTHOR INFORMATION

Corresponding Author

*Fax:+82-2-364-7050. E-mail: esim@yonsei.ac.kr.

Notes

The authors declare no competing financial interest.

ACKNOWLEDGMENTS

This work was supported by the national research foundation (NRF) grant funded by the Korea government (2011-0002832, 2011-0003690, and 2010-220-C00017). M.H. thanks the fellowship of the BK 21 program from MOEHRD.

REFERENCES

(1) Discher, D. E.; Eisenberg, A. *Science* **2002**, *297*, 967−973.
(2) Davis, M. E.; Chen, Z.; Shin, D. M. *Nat. Rev. Drug Discovery* **2008**, *7*, 771−782.
(3) Jain, J. P.; Kumar, N. *Biomacromolecules* **2010**, *11*, 1027−1035.
(4) Petros, R. A.; DeSimone, J. M. *Nat. Rev. Drug Discovery* **2010**, *9*, 615−627.
(5) Mishra, B. K.; Thomas, B. N. *J. Am. Chem. Soc.* **2002**, *124*, 6866−6871.
(6) Jin fan, H.; Knez, M.; Scholz, R.; Nielsch, K.; Pippel, E.; Hesse, D.; Zacharias, M.; Gosele, U. *Nat. Mater.* **2006**, *5*, 627−631.
(7) Shimizu, T. *J. Polym. Sci., Part A: Polym. Chem.* **2006**, *44*, 5137−5152.
(8) Tarabout, C.; Roux, S.; Gobeaux, F.; Fay, N.; Pouget, E.; Meriadec, C.; Ligeti, M.; Thomas, D.; IJsselstijn, M.; Besselievre, F. *Proc. Natl. Acad. Sci. U.S.A.* **2011**, *108*, 7679−7684.
(9) Wang, B.; Poa, C. H. P.; Wei, L.; Li, L.-J.; Yang, Y.; Chen, Y. *J. Am. Chem. Soc.* **2007**, *129*, 9014−9019.
(10) Leila, Z. *J. Controlled Release* **2002**, *81*, 7−23.
(11) Li, Y. D.; Li, X. L.; He, R. R.; Zhu, J.; Deng, Z. X. *J. Am. Chem. Soc.* **2002**, *124*, 1411−1416.
(12) Son, S. J.; Bai, X.; Nan, A.; Ghandehari, H.; Lee, S. B. *J. Controlled Release* **2006**, *114*, 143−152.
(13) Fan, H. J.; Gösele, U.; Zacharias, M. *Small* **2007**, *3*, 1660−1671.
(14) Lee, E.; Kim, J.-K.; Lee, M. *Angew. Chem., Int. Ed.* **2009**, *121*, 3711−3714.
(15) Radzihovsky, L.; Toner, J. *Phys. Rev. Lett.* **1995**, *75*, 4752−4755.
(16) Bowick, M.; Falcioni, M.; Thorleifsson, G. *Phys. Rev. E* **1997**, *79*, 885−888.
(17) Stenull, O. *Phys. Rev. E* **2008**, *78*, 031704.
(18) Johnson, D. L.; Esmen, N. A.; Carlson, K. D.; Pearce, T. A.; Thomas, B. N. *J. Aerosol Sci.* **2000**, *31*, 181−188.
(19) Iijima, S.; Brabec, C.; Maiti, A.; Bernholc, J. *J. Chem. Phys.* **1996**, *104*, 2089−2092.
(20) Baughman, R. H.; Zakhidov, A. A.; de Heer, W. A. *Science* **2002**, *297*, 787−792.
(21) Meyer, J. C.; Geim, A. K.; Katsnelson, M. I.; Novoselov, K. S.; Booth, T. J.; Roth, S. *Nature* **2007**, *446*, 60−63.
(22) Wen, X.; Garland, C. W.; Hwa, T.; Kardar, M.; Kokufuta, E.; Li, Y.; Orkisz, M.; Tanaka, T. *Nature* **1992**, *355*, 426−428.
(23) Spector, M. S.; Naranjo, E.; Chiruvolu, S.; Zasadzinski, J. A. *Phys. Rev. Lett.* **1994**, *73*, 2867−2870.
(24) Stupp, S. I.; Son, S.; Lin, H. C.; Li, L. S. *Science* **1993**, *259*, 59−63.
(25) Endo, H.; Kado, Y.; Mitsuishi, M.; Miyashita, T. *Macromolecules* **2006**, *39*, 5559−5563.
(26) Eck, W.; Kuller, A.; Grunze, M.; Volkel, B.; Golzhauser, A. *Adv. Mater.* **2005**, *17*, 2583−2587.
(27) Knauert, S. T.; Douglas, J. F.; Starr, F. W. *Macromolecules* **2010**, *43*, 3438−3445.
(28) Han, M.; Sim, E. *J. Phys. Chem. B* **2012**, *116*, 1796−1801.
(29) Hong, D.-J.; Lee, E.; Jeong, H.; Lee, J.-k.; Zin, W.-C.; Nguyen, T. D.; Glotzer, S. C.; Lee, M. *Angew. Chem., Int. Ed.* **2009**, *48*, 1664−1668.
(30) Frenkel, D.; Smit, B. *Understanding Molecular Simulation*; Academic Press: San Diego, CA, 2002.
(31) Han, M.; Hong, M.; Sim, E. *J. Chem. Phys.* **2011**, *134*, 204901.
(32) http://lammps.sandia.gov.
(33) Humphrey, W.; Dalke, A.; Schulten, K. *J. Mol. Graphics* **1996**, *14*, 33−38.
(34) Groot, R. D.; Rabone, K. L. *Biophys. J.* **2001**, *81*, 725−736.
(35) Fujie, T.; Park, J. Y.; Murata, A.; Estillore, N. C.; Tria, M. C. R.; Takeoka, S.; Advincula, R. C. *ACS Appl. Mater. Interfaces* **2009**, *1*, 1404−1413.
(36) Fujie, T.; Matsutani, N.; Kinoshita, M.; Okamura, Y.; Saito, A.; Takeoka, S. *Adv. Funct. Mater.* **2009**, *19*, 2560−2568.
(37) Knoll, W.; Advincula, R. C. *Functional Polymer Films*, 1st ed.; Wiley-VCH: Weinheim, 2011.
(38) Zimmerberg, J.; Kozlov, M. M. *Nat. Rev. Mol. Cell Biol.* **2006**, *7*, 9−19.
(39) Campelo, F.; McMahon, H. T.; Kozlov, M. M. *Biophys. J.* **2008**, *95*, 2325−2339.
(40) Hong, D.-J.; Lee, E.; Lee, J.-K.; Zin, W.-C.; Han, M.; Sim, E.; Lee, M. *J. Am. Chem. Soc.* **2008**, *130*, 14448−14449.
(41) Horsch, M. A.; Zhang, Z.; Glotzer, S. C. *Nano Lett.* **2006**, *6*, 2406−2413.
(42) Berg, J. M.; Tymoczko, J. L.; Stryer, L. *Biochemistry*, 7th ed.; W.H. Freeman & Co. Ltd.: New York, 2011.